Sulfur metabolic response in macrophage limits excessive inflammatory response by creating a negative feedback loop

Takeda, Haruna

Murakami, Shohei

Liu, Zun

Sawa, Tomohiro

他

出版情報：Redox Biology. 65, pp.102834-, 2023-09. Elsevier
バージョン：

Redox Biology 65 (2023) 102834

Contents lists available at ScienceDirect

Redox Biology

journal homepage: www.elsevier.com/locate/redox

Research Paper

Sulfur metabolic response in macrophage limits excessive inflammatory response by creating a negative feedback loop

Haruna Takeda [a], Shohei Murakami [a], Zun Liu [a], Tomohiro Sawa [b], Masatomo Takahashi [c], Yoshihiro Izumi [c], Takeshi Bamba [c], Hideyo Sato [d], Takaaki Akaike [e], Hiroki Sekine [a], Hozumi Motohashi [a,*]

[a] Department of Gene Expression Regulation, Institute of Development, Aging and Cancer, Tohoku University, Sendai, 980-8575, Japan
[b] Department of Microbiology, Graduate School of Medical Sciences, Kumamoto University, 1-1-1 Honjou, Kumamoto, 860-8556, Japan
[c] Division of Metabolomics/Mass Spectrometry Center, Medical Research Center for High Depth Omics, Medical Institute of Bioregulation, Kyushu University, Fukuoka, 812-8582, Japan
[d] Department of Medical Technology, Faculty of Medicine, Niigata University, Niigata, 951-8518, Japan
[e] Department of Environmental Medicine and Molecular Toxicology, Tohoku University Graduate School of Medicine, Sendai, 980-8575, Japan

ARTICLE INFO

Keywords:
Macrophage
Cysteine
xCT
Inflammation
Persulfide
LPS

ABSTRACT

The excessive inflammatory response of macrophages plays a vital role in the pathogenesis of various diseases. The dynamic metabolic alterations in macrophages, including amino acid metabolism, are known to orchestrate their inflammatory phenotype. To explore a new metabolic pathway that regulates the inflammatory response, we examined metabolome changes in mouse peritoneal macrophages (PMs) in response to lipopolysaccharide (LPS) and found a coordinated increase of cysteine and its related metabolites, suggesting an enhanced demand for cysteine during the inflammatory response. Because *Slc7a11*, which encodes a cystine transporter xCT, was remarkably upregulated upon the pro-inflammatory challenge and found to serve as a major channel of cysteine supply, we examined the inflammatory behavior of *Slc7a11* knockout PMs (xCT-KO PMs) to clarify an impact of the increased cysteine demand on inflammation. The xCT-KO PMs exhibited a prolonged upregulation of pro-inflammatory genes, which was recapitulated by cystine depletion in the culture media of wild-type PMs, suggesting that cysteine facilitates the resolution of inflammation. Detailed analysis of the sulfur metabolome revealed that supersulfides, such as cysteine persulfide, were increased in PMs in response to LPS, which was abolished in xCT-KO PMs. Supplementation of N-acetylcysteine tetrasulfide (NAC-S2), a supersulfide donor, attenuated the pro-inflammatory gene expression in xCT-KO PMs. Thus, activated macrophages increase cystine uptake via xCT and produce supersulfides, creating a negative feedback loop to limit excessive inflammation. Our study highlights the finely tuned regulation of macrophage inflammatory response by sulfur metabolism.

1. Introduction

Macrophages are immune cells of hematopoietic origin with versatile functions such as development, homeostasis and repair, and immune responses against pathogens [1]. When tissues are damaged by infection or injury, inflammatory monocytes are recruited from the circulation and differentiated into macrophages. These macrophages often show a proinflammatory phenotype, secreting various inflammatory mediators such as IL-1, IL-6, IL-12, and prostaglandins [2]. These inflammatory processes are initially beneficial because they facilitate the clearance of invading organisms. However, once prolonged, they also trigger collateral tissue damage via reactive oxygen and nitrogen species, which are involved in the pathogenesis of chronic inflammatory and autoimmune diseases [3].

Recent studies have demonstrated that this pro-inflammatory process couples dynamic metabolic reprogramming, such as enhanced glycolysis, accumulation of itaconate and succinate, biosynthesis of fatty acids from citrate, and decreased oxidative phosphorylation [4]. This dynamic metabolic reprogramming not only supports their energetic demands but also allows production of metabolites that mediate specific signaling cascades, which promote both initiation and resolution of inflammation [5–11].

* Corresponding author.
E-mail address: hozumi.motohashi.a7@tohoku.ac.jp (H. Motohashi).

https://doi.org/10.1016/j.redox.2023.102834
Received 17 June 2023; Received in revised form 24 July 2023; Accepted 28 July 2023
Available online 29 July 2023

Amino acids are one of the key players in metabolic alteration. The divergent immunomodulatory axis shaped by different amino acids emphasizes their requirement beyond protein translation. For instance, in LPS-challenged macrophages, inducible nitric oxide synthase (iNOS) facilitates arginine conversion to nitric oxide, which participate in inflammasome activation [12] or dampening OXPHOS capacity by protein nitrosylation [13]. On the other hand, recent reports demonstrated that serine biosynthesis is required for *Il1b* mRNA expression [14]. The discovery of these finely tuned metabolic communications prompted us to decipher another regulatory axis that orchestrates the inflammatory milieu.

Among various amino acids, cysteine plays a critical role in cellular redox regulation. Cysteine is synthesized from methionine via the transsulfuration pathway, in which cystathionine beta-synthase (CBS) and cystathionine gamma-lyase (CGL) are involved. Another supply route is via cystine transported by xCT, a transmembrane sodium-independent and chloride-dependent antiporter of cystine and glutamate [15,16]. The transported cystine is reduced to cysteine in cells and used for glutathione synthesis and protein translation. More recently, it has been demonstrated that a substantial portion of sulfur metabolites contain sulfane sulfur and polymeric sulfur, *i.e.,* catenated sulfur, such as in cysteine persulfide and glutathione trisulfide [17,18]. The inorganic and organic sulfur with sulfur catenation is called supersulfides (RSSnH, $n > 1$, R = hydrogen or alkyl), which have been recognized as a new entity of biomolecules involved in various biological processes including antioxidant function [18], anti-inflammatory function [19], signal transduction [20], and mitochondrial activation [17,21]. Although previous studies reported that xCT-deficient peritoneal macrophages (xCT-KO PMs) exhibit impaired nitric oxide production and decreased viability after long-term culture [22,23], suggesting substantial requirement of cysteine for macrophage function, how sulfur metabolites, including supersulfides, impact macrophage behavior remains to be elucidated.

In this study, we explored a novel metabolic pathway that regulates the inflammatory response of macrophages and found a remarkable increase in cysteine demand during the inflammatory response with the emergence of a critical role of supersulfides in terminating the response. Sulfur metabolism involves metabolic rewiring that regulates the inflammatory process of macrophages and creates a negative feedback loop to limit excessive inflammation.

2. Materials and methods

2.1. Mice

2-5 months-old wild-type (WT) and *Slc7a11* knockout (xCT-KO) mice on a C57BL/6 J background were used in this study [24]. Both males and females were included in the analysis because phenotypic differences of PMs were indistinguishable between males and females. All mice were housed in specific pathogen-free conditions according to the regulations of The Standards for Human Care and Use of Laboratory Animals of Tohoku University and the Guidelines for Proper Conduct of Animal Experiments by the Ministry of Education, Culture, Sports, Science, and Technology of Japan. The permission codes for the animal experiment were 2021AcA-002.

2.2. Reagents

DL-Buthionine-(*S*,*R*)-sulfoximine (BSO) was purchased from Sigma-Aldrich (MO, USA). OxNAC and NAC-S2 were prepared as previously described [19]. Glutathione trisulfide (GSSSG) was prepared as previously described [21].

2.3. Preparation of peritoneal exudate macrophages (PMs)

To collect peritoneal exudate macrophages (PMs), mice were intraperitoneally injected with 2 mL of 4% thioglycolate. Peritoneal cells were isolated from exudates in the peritoneal cavity three days after the injection and incubated in cell culture plates for over 1 h. After washing two times with PBS, the adherent cells were cultured as PMs in DMEM supplemented with penicillin-streptomycin and 10% FBS at 37 °C in 5% CO_2 and used for experiments. For all experiments except for RNA-seq analysis, we prepared the replicates from individual mice collected on at least three different days. For RNA-seq analysis, we prepared two replicates from individual mice collected on two different days. PM viability was assessed using the CytoTox-ONE™ homogeneous membrane integrity assay (Promega) and verified to be unaffected by 24 h of LPS treatment, cystine depletion, BSO treatment, NAC-S2 treatment, or oxNAC treatment.

2.4. LPS treatment of macrophages

PMs were stimulated with 100 ng/mL LPS from Escherichia coli 0111: B4 (Sigma-Aldrich). PMs were harvested for RNA purification and mass spectrometry analysis at indicated time points.

2.5. Manipulation of cystine content in the medium

Custom-ordered DMEM (Low-Glucose) without cystine and phenol red was purchased from Cell Science & Technology Institute (Miyagi, Japan). Prior to the experiment, cystine-deficient medium (0 μM), cystine-limited medium (20 μM), and cystine-sufficient medium (200 μM) were prepared by adding appropriate volumes of 100 mM cystine dissolved in 2 M HCl to the custom-ordered DMEM with an equivalent volume of 2 M NaOH. Upon LPS stimulation, the culture medium of PMs was changed to that containing cystine at a concentration of 0, 20, or 200 μM.

2.6. Targeted metabolome analysis

The Bligh and Dyer method was utilized with minor modifications to extract total metabolites from PMs [25]. PMs were washed twice with cold PBS and harvested in 1 mL cold methanol (−30 °C) containing 10-camphor sulfonic acid (1.5 nmol) and piperazine-1,4-bis (2-ethane sulfonic acid) (PIPES) (1.5 nmol) as internal standards (ISs). The samples were vortexed for 1 min and sonicated for 5 min to ensure thorough mixing, followed by incubation on ice for 5 min to precipitate protein. After centrifugation at 16,000 g for 5 min at 4 °C, the supernatant was collected, and the protein concentrations in the pellet were determined using a pierce™ BCA Protein Assay Kit. Then, 600 μL of supernatant was mixed with an equivalent volume of chloroform and 480 μL of water, and the upper layer (800 μL) was collected after centrifugation at 16,000 g and 4 °C for 5 min for hydrophilic metabolite analysis. For the analysis of anionic polar metabolites such as succinate, lactate, and PLP, ion chromatography (Dionex ICS-5000$^+$ HPIC system, Thermo Fisher Scientific) with a Dionex IonPac AG11-HC-4 μm guard column (2 mm i. d. × 50 mm, 4 μm particle size, Thermo Fisher Scientific) and a Dionex IonPac AS11-HC-4 μm column (2 mm i. d. × 250 mm, 4 μm particle size, Thermo Fisher Scientific) coupled with a Q Exactive, high-performance benchtop quadrupole Orbitrap high-resolution tandem mass spectrometer (Thermo Fisher Scientific) (IC/HRMS/MS) [25] were utilized. On the other hand, cationic polar metabolites were analyzed through liquid chromatography (Nexera X2 UHPLC system, Shimadzu Co., Kyoto, Japan) with a Discovery HS F5 column (2.1 mm i. d. × 150 mm, 3 μm particle size, Merck) coupled with a Q Exactive instrument (PFPP-LC/HRMS/MS) [25].

2.7. RNA-seq analysis

Total RNA was extracted from PMs using the RNeasy Mini Kit (Qiagen) in biological duplicates. After performing quality control, libraries were constructed from total RNA using TruSeq Stranded mRNA

LT Sample Prep Kit according to the manufacturer's protocol (TruSeq Stranded mRNA Sample Preparation Guide, Part # 15031047 Rev. E). Briefly, the sequencing library was created by randomly fragmenting the cDNA sample, followed by 5′ and 3′ adapter ligation. Adapter-ligated fragments were then purified through PCR amplification and gel electrophoresis. The libraries were then sequenced on an Illumina platform, generating 102-base pair-end reads. The BCL (base calls) binary was then transformed into FASTQ format using the bcl2fastq package developed by Illumina. All these procedures above, except for RNA purification, were conducted by Macrogen Japan (Kyoto, Japan).

After obtaining raw fastq sequencing files, fastp version 0.20.1 was conducted to check the quality and trim possible adapters, poly-A tails, and low-sequence quality bases. After trimming, all the remaining reads were aligned to the Grcm39 reference genome using STAR version 2.7.8a. After mapping, RSEM version 1.3.3 was used to calculate each gene's raw read counts and TPM (Transcripts Per Kilobase Million) value.

2.8. Data analysis of RNA-seq results

Raw output data generated by RSEM were transferred to RStudio (ver. 2022.07.1 Build 554). Among 55414 genes quantified, those with extremely low counts (Means of all samples were four or below) were eliminated, and 14926 genes were retained for further analysis.

Raw read counts were used to define and analyze differentially expressed genes (DEGs). Pseudo count (+1) was added to the raw read count of an individual gene. To calculate an AUC value, the raw count data of an individual gene at each time point were summed. Comparison between data of 0 μM cystine and those of 200 μM cystine at each time point or area under curve (AUC) was made by Wald-test using DEseq2 (ver. 1.34.0) with default parameters. Genes with adjusted p values < 0.05 and $|\log_2 FC| > 1$ (FC: fold change of 0 μM vs. 200 μM) were considered DEGs. After DEseq2 calculation, the ENSEMBL gene names were converted to external gene names using biomaRt (ver. 2.50.3) and visualized as a volcano plot and heatmap using ggplot2 (ver. 3.3.6) and Pheatmap (ver. 1.0.12), respectively. Enrichment analysis was performed by the "enricher" function in the clusterProfiler package (ver. 4.2.2), with gmt files downloaded from Enrichr (https://maayanlab.cloud/Enrichr/) as input. The results were visualized as bar plots using ggplot2.

TPM values of the 14926 genes selected above were used for the principal component analysis. The "Prcomp" function was run, and PC1 and PC2, with the Proportion of Variance of each component, were visualized as a scatter plot using ggplot2.

2.9. ELISA

PMs were seeded at 1 x 10^5 cells/well in 96-well plates, incubated with 100 ng/mL LPS for 24 h, and further incubated for 2 h with 5 mM ATP. Culture supernatants were collected and used for IL-1β measurement after proper dilution using mouse IL-1β ELISA kits (R&D Systems).

2.10. RNA purification and quantitative RT-PCR

According to the manufacturer's instructions, total RNA samples were prepared from PMs using ISOGEN (Nippon Gene) or ReliaPrep™ RNA Miniprep Systems (Promega). First-strand cDNA was synthesized from 100 ng of total RNA using ReverTra Ace qPCR RT Master Mix with gDNA Remover (TOYOBO). Real-time PCR was performed for each sample with QuantStudio RT-PCR system (Thermo Fisher Scientific, Waltham, MA, USA) using KAPA SYBR FAST qPCR Master Mix (Kapa Biosystems, Wilmington, MA, USA). *Hprt* (hypoxanthine phosphoribosyl transferase 1) gene expression levels were used as internal controls for normalization. The primer sets used in the RT-PCR are listed in Supplementary Table S1.

2.11. Measurement of total glutathione

PMs were seeded in 24-well plates and incubated with or without LPS and BSO for 12–24 h. After washing with Wash buffer (0.1 M phosphate buffer containing 5 mM EDTA) twice, 100 μL of Lysis buffer (0.1 M phosphate buffer containing 5 mM EDTA and 0.1% Triton X-100) was added to the wells. After incubation for 5 min, 15 μL of 0.1 N hydrogen chloride and an equivalent amount of 5% 5-sulfosalicylic acid were added to the well and collected into the tubes. After centrifugation for 5 min at 15,000 rpm, 4 °C, supernatants were used for the subsequent analysis. Cellular total glutathione was measured by Total Glutathione Quantification Kit (DOJINDO Molecular Technologies, Tokyo, Japan) based on the GSH-reductase mediated enzyme recycling method together with the Ellman's reagent, DTNB [5,5′-dithiobis (2-nitrobenzoic acid)], according to the manufacturer's instruction. The absorbance of 410 nm light for produced 5-mercapto-2-nitrobenzoic acid was measured.

2.12. Sulfur metabolome analysis

Sulfur metabolites were measured by the method based on alkylation with β-(4-hydroxyphenyl) ethyl iodoacetamide (HPE-IAM), followed by LC-ESI-MS/MS analysis, as shown in the previous studies [17,26]. Briefly, 1 × 10^6 cells were washed twice with PBS, frozen by liquid nitrogen and stored at −80 °C until analysis. The cells were lysed with 70% methanol solution containing 5 mM HPE-IAM and 50 mM sodium acetate (pH 6.5) and sonicated for complete lysis. The lysates were incubated at 37 °C for 20 min, followed by centrifugation at 14,000 g for 10 min at 4 °C. The supernatants were acidified with an equivalent amount of 0.1% formic acid (FA). Through this alkylation of sulfur metabolites, hydropersulfides and hydropolysulfides were detected as HPE-IAM adducts, and oxidized persulfides/polysulfides were detected as natural forms. The pellets were dissolved in 0.1% SDS/PBS, and protein content was measured by BCA assay.

For quantification of sulfur metabolites by liquid chromatography-electrospray ionization-tandem mass spectroscopy (LC-ESI-MS/MS), isotope-labeled internal standards [17,26] (Supplementary Table S2) were spiked into the samples; the final concentration of each standard for the reduced metabolites was 25 nM, and that for the oxidized metabolites was 250 nM. The samples premixed with the internal standards were analyzed with a triple quadrupole mass spectrometer LCMS-8060 (SHIMADZU) coupled to a Nexera UHPLC system (SHIMADZU). For the measurement of reduced metabolites, the samples were separated by means of the Nexera UHPLC system with a YMC-Triart C18 (50 × 2.0 mm, 3 μm) column under the following linear gradient: mobile phase A (0.1% FA) was decreased against mobile phase B (0.1% FA in 100% methanol) from 97% to 5% for 12 min at a flow rate of 0.2 ml/min at 40 °C. For the measurement of oxidized metabolites, the samples were separated by means of the Nexera UHPLC system with an Intrada Amino Acid (100 × 3.0 mm, 3 μm) column under the following linear gradient: mobile phase A (0.1% FA in 100% acetonitrile) was decreased against mobile phase B (100 mM ammonium formate) from 25% to 75% for 15 min at a flow rate of 0.5 ml/min at 40 °C. The MRM parameters shown in the previously published work [17] were used to identify each compound, with a modification of the cystine and CysSSSCys parameters shown in Supplementary Table S2.

2.13. Statistical analysis

All statistical analyses, except for RNA-seq and metabolome analysis, were conducted using Prism 9 (GraphPad Software, CA, USA). Data were presented as mean ± S.E.M. and tested with one-way or two-way analysis of variance (ANOVA) followed by Tukey's multiple comparison test. The *P*-value of <0.05 was considered significant.

3. Results

3.1. LPS treatment increases cysteine-related metabolites in macrophages

To explore a new metabolic pathway that regulates the inflammatory response of macrophages, we conducted a metabolome analysis of mouse PMs treated with LPS. PMs were harvested 8 and 24 h after LPS treatment, and metabolite levels were compared with those before the LPS treatment (Fig. 1). Among 172 metabolites, 18 metabolites were significantly increased 24 h after LPS treatment (Fold Change >1.5 & P-value <0.05) (Fig. 1A and B). Consistent with previous reports, the increased metabolites included itaconate and succinate, which are known as immunometabolites regulating immune cell functions and inflammatory processes (Fig. 1A) [8,9]. Intriguingly, we noticed that cysteine-derived metabolites, oxidized and reduced glutathione, cysteine sulfinic acid, and γ-glutamylcysteine, were also increased (Fig. 1B), which led us to assume that cysteine is actively involved in the inflammatory response in macrophages. When the metabolome data were re-evaluated for cysteine-related metabolites, cysteine, and cysteic acid were found marginally increased. The transsulfuration pathway intermediates, S-adenosylhomocysteine and S-adenosylmethionine, showed similar tendencies. An exception was homocysteic acid, which tended to be decreased (Fig. 1B and C). These results suggest that stimulated macrophages increase their demand for cysteine.

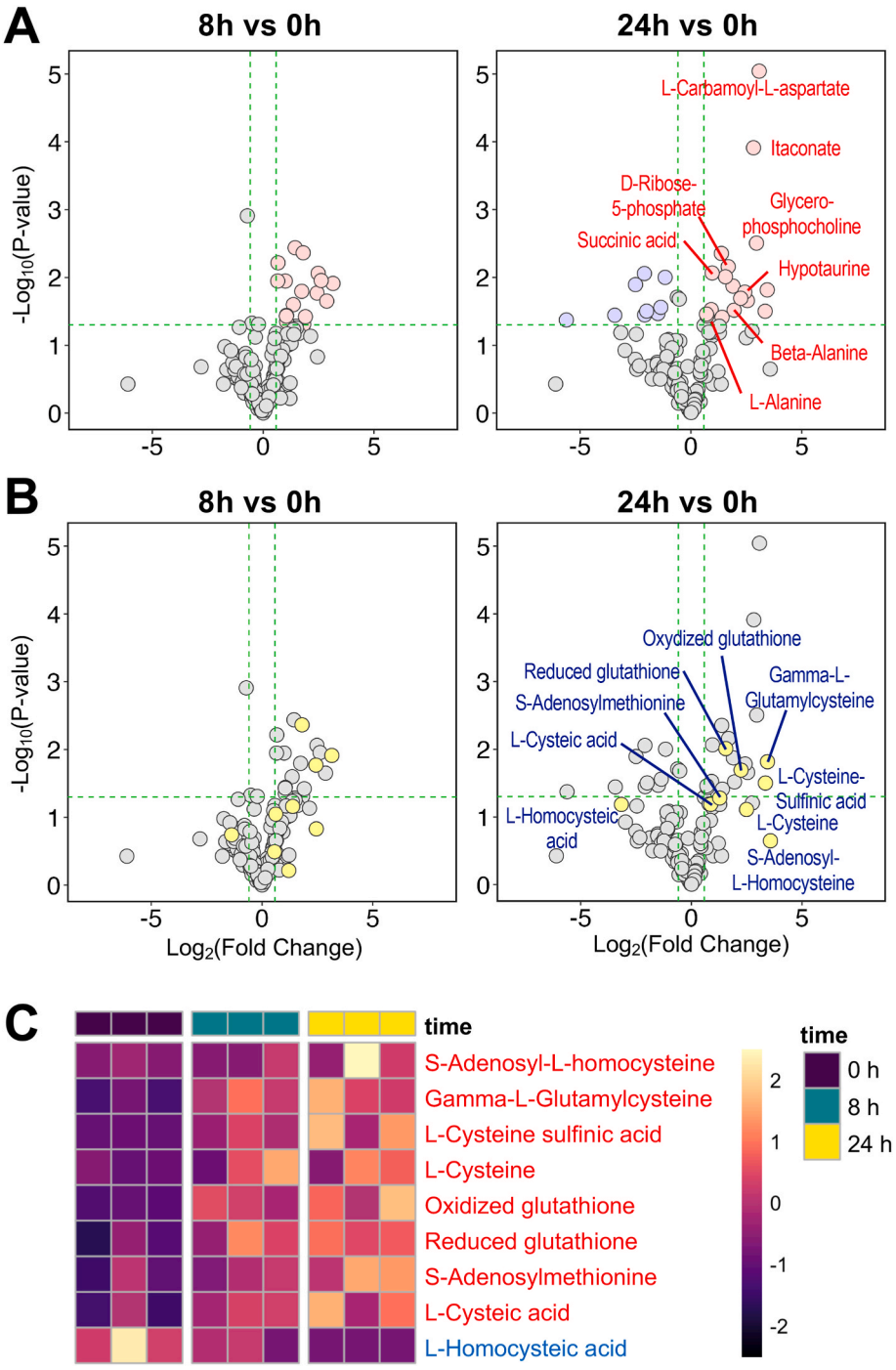

Fig. 1. Metabolomic landscape of LPS-treated macrophages.
(**A, B**) Metabolome analysis was conducted using PMs stimulated with LPS for 0, 8, and 24 h. Volcano plots of metabolites at 8 h (left panel) and 24 h (right panel) after the LPS treatment, respectively, compared with those of non-treated groups (0 h). Increased and decreased metabolites at each time point after LPS treatment are shown in red and blue, respectively (**A**). Sulfur metabolites are shown in yellow (**B**). Green vertical lines denote fold change = 1.5 or 1/1.5, while the horizontal line denotes P-value = 0.05. P-values were calculated by Student's *t*-test. (**C**) Heatmap showing abundance of each sulfur metabolite in individual replicates (n = 3). Increased and decreased metabolites by LPS treatment are shown in red and blue, respectively. (For interpretation of the references to colour in this figure legend, the reader is referred to the Web version of this article.)

3.2. Cystine transporter xCT plays a major role to meet the increased cysteine demand of proinflammatory macrophages

We found that expression of *Slc7a11*, which encodes a cystine transporter xCT, is remarkably elevated upon LPS treatment (Fig. 2A), implying that cystine uptake is strongly facilitated in macrophages during the inflammatory response. In contrast, expression levels of transsulfuration enzyme genes, *Cth* and *Cbs*, are only modestly upregulated and not detected, respectively (Fig. 2B and data not shown). Thus, extracellular cystine rather than methionine via transsulfuration was expected to be a major source of cysteine during the inflammatory response of macrophages.

Based on these results, we examined xCT-deficient PMs collected from *Slc7a11*-deficient (xCT-KO) mice to examine the functional significance of the increased cysteine demand during the inflammatory response of macrophages. Lack of *Slc7a11* expression was verified in xCT-KO PMs (Fig. 2A). Wild-type (WT) and xCT-KO PMs was harvested before and after the LPS treatment for metabolome analysis (Fig. 2C). Consistent with a very low expression level of *Slc7a11* in WT PMs before the LPS treatment, a metabolome profile of xCT-KO PMs was almost comparable with that of WT PMs (Fig. 2C, left panel). A small number of metabolites were differentially detected after 8 h of the LPS treatment (Fig. 2C, middle panel), and an increased number of metabolites were differentially detected after 24 h of the LPS treatment (Fig. 2C, right panel), which was likely to be explained by the incrementally increased xCT contribution according to the increased *Slc7a11* expression induced by the LPS treatment.

As we expected, the differentially detected metabolites included cysteine and its related metabolites. Cysteine and its oxidized forms, cysteine sulfinic acid and cysteic acid, and glutathione and its precursors, gamma-glutamylcysteine, oxidized glutathione, and reduced glutathione, were remarkably reduced in xCT-KO PMs, most prominently at 24 h after LPS treatment (Fig. 2D and E). On the other hand, among transsulfuration pathway intermediates, S-adenosylmethionine, S-adenosylhomocysteine, and homocysteic acid, did not show any clear coordinate changes (Fig. 2F). Although *Cth* expression was remarkably upregulated in xCT-KO PMs (Fig. 2B), transsulfuration pathway did not compensate the cysteine depletion in xCT-KO PMs probably due to lack of *Cbs* expression in macrophages. Interestingly, homocysteic acid was decreased in response to LPS in xCT-dependent manner (Fig. 2F). We speculate that structural similarities of homocysteic acid and glutamic acid might have allowed xCT to export homocysteic acid when LPS treatment increased xCT expression.

As for the significantly increased metabolites in xCT-KO PMs, glutamate, aspartate, asparagine, and phosphoserine were listed (Supplementary Figs. S1A and S1B). The increase in glutamate was likely to result from the xCT deficiency, which serves as an antiporter of cystine and glutamate. The increase of aspartate, asparagine, and phosphoserine implied the facilitation of asparagine synthesis and serine synthesis (Supplementary Figs. S1C and S1D). Consistently, genes encoding a key enzyme for asparagine synthesis, asparagine synthetase (ASNS), and one of the serine synthesis pathway enzymes, phosphoserine aminotransferase 1 (PSAT1), were upregulated in xCT-KO PMs (Supplementary Fig. S1E). We suspected that this was due to the activation of the ATF pathway as ATF is known to regulate *Asns* and genes for the serine synthesis (*Phgdh*, *Psat1*, *Psgh*) together with *Cth* (Fig. 2B). Indeed, more abundant nuclear accumulation of ATF4 protein was observed in xCT-KO PMs than WT PMs (Supplementary Fig. S1F), suggesting that the amino acid starvation response is triggered due to the unavailability of cystine in xCT-KO PMs despite the increased cysteine demand during the inflammatory response, resulting in the consequent activation of ATF4.

Collectively, these data highlighted the altered metabolite profiles, especially in sulfur metabolites, in xCT-KO PMs and thus clarified that extracellular cystine is an essential source of cysteine through cystine transporter xCT after the LPS challenge.

3.3. Inflammatory response is amplified in xCT-deficient macrophages

We next investigated how the inflammatory response of macrophages is affected when the cysteine demand is not satisfied. The expression of representative inflammatory genes was examined in xCT-KO PMs after the LPS treatment (Fig. 3A-E). *Il1b, Il1a, Il12a, Il6*, and *Ptgs2* expression levels were all elevated in xCT-KO PMs than WT PMs. The difference was apparent, especially in the later stage, suggesting that cystine uptake via xCT is necessary for the resolution of the inflammatory response by terminating the transcriptional activation of the inflammatory genes. In addition, xCT-KO PMs secreted a remarkably increased amount of IL-1β into the medium (Fig. 3F), which was much more robust than the increased mRNA level of the *Il1b* gene (Fig. 3A). As the secretion of IL-1β needs posttranslational processing by the inflammasome, the cysteine availability is likely to support the inflammasome activity. These data demonstrate that macrophages challenged with LPS augment xCT-dependent cystine uptake and that the cystine contributes to the resolution of inflammatory response via regulation of the inflammatory gene transcription and inflammasome activity.

3.4. Limitation of cystine supply enhances the pro-inflammatory phenotype of macrophages

To further verify the importance of extracellular cystine uptake for control of the macrophage inflammatory response, we examined the effect of limitation of the extracellular cystine on the proinflammatory gene expression (Fig. 4A-E). When cystine was depleted from the culture medium, PMs were not subjected to ferroptosis but exhibited enhanced pro-inflammatory gene expression in response to LPS, which is similar to the result observed in xCT-KO PMs (see Fig. 3A-E). The secretion of IL-1β was increased by cystine depletion (Fig. 4F), which is also similar to the result observed in xCT-KO PMs (see Fig. 3F).

For comprehensive understanding of the transcriptional landscape influenced by the availability of extracellular cystine, we conducted RNA-sequencing analysis of PMs stimulated with LPS in the presence or absence of cystine in the culture medium. The PMs were harvested 2, 4, 8, 12, and 24 h after the LPS treatment/cystine depletion, and fold changes of gene expression in the absence vs. presence of cystine were calculated at each time point (Fig. 4G). The number of differentially expressed genes was incrementally increased in a time-dependent manner: only 7 genes after 2 h of the LPS treatment/cystine depletion, whereas 60, 508, 1404, and 1810 genes were differentially expressed after 4, 8, 12, and 24 h of the LPS treatment/cystine depletion, respectively, out of 14926 genes tested (Supplementary Table S3). The impacts of cystine depletion in the culture medium became gradually larger, which is likely to reflect the increased requirement of cystine during the inflammatory response. The principal component analysis confirmed the substantial overall transcriptomic changes (Fig. 4H).

To identify genes whose expression levels are significantly altered over the time course examined, we approximated the total expression level of a gene by calculating its area under the curve (AUC) from the expression level at each time point (Fig. 4I and Supplementary Fig. S2A). 1014 and 1297 genes were identified as differentially upregulated and downregulated genes, respectively (Fig. 4I and Supplementary Fig. S2A). Pathway analysis based on the GO biological process database revealed that cytokine-mediated signaling pathway and defense response to the virus were significantly enriched in upregulated genes (Fig. 4J), whereas genes related to extracellular matrix organization were significantly enriched in downregulated genes (Supplementary Fig. S2B). Consistently, enrichment analysis based on the ChEA database revealed that genes bound by RELA, IRF8, and STAT3, which are all closely related to the pro-inflammatory cytokine production, were enriched among upregulated genes (Fig. 4K). Besides the genes examined in Fig. 4A-F, upregulation was observed for genes encoding many other pro-inflammatory genes (Fig. 4L). Taken together, these data revealed that cystine depletion augments proinflammatory phenotypes

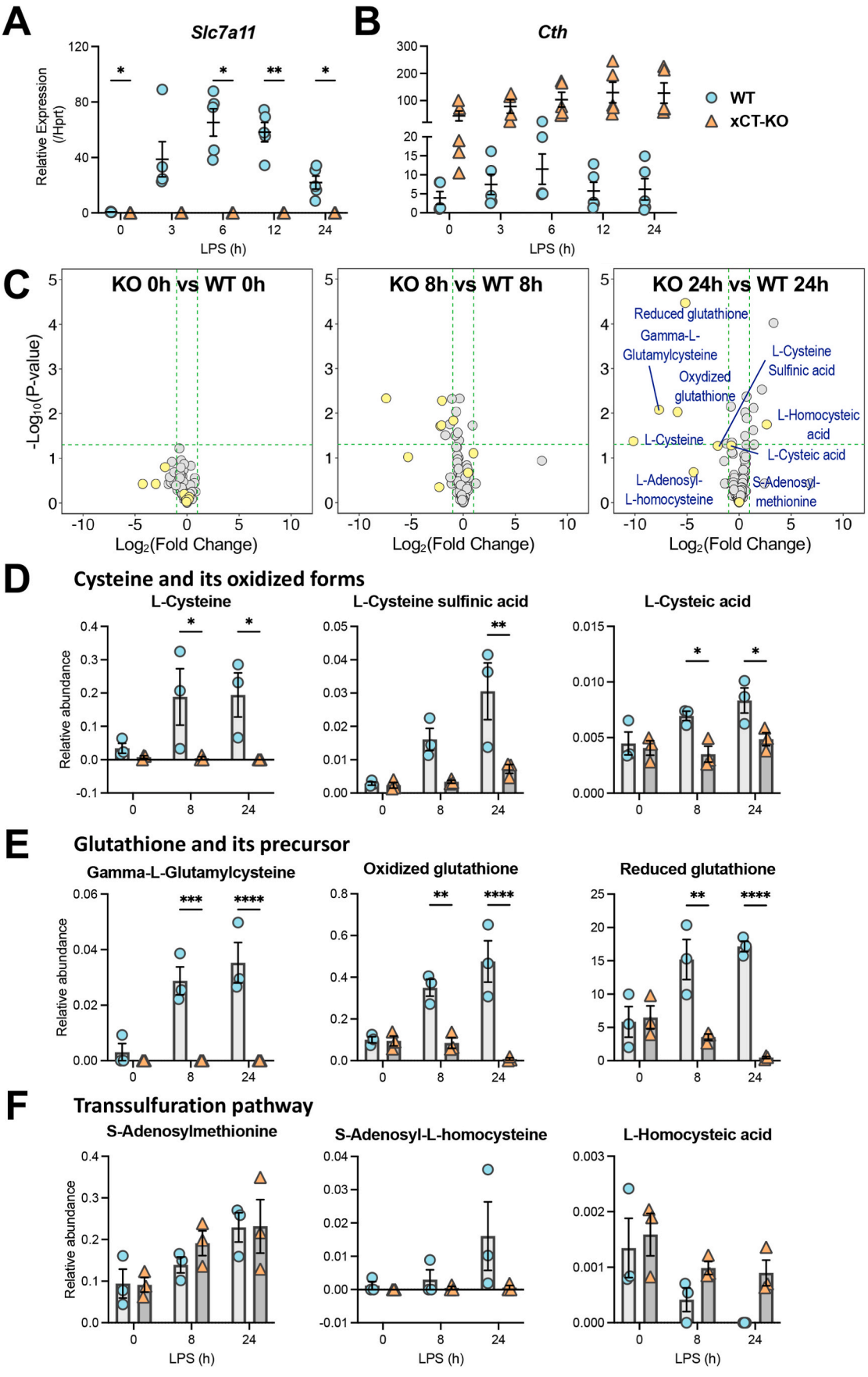

(caption on next page)

Fig. 2. Decreased metabolites in xCT-KO PMs during inflammatory response.
(**A, B**) RT-PCR quantification of mRNA levels of *Slc7a11* (**A**) and *Cth* (**B**) in WT and xCT-KO PMs stimulated with 100 ng/μL LPS for indicated time (n = 4–5). Error bars represent S.E.M. of 4–5 replicates. Two-way ANOVA was conducted to evaluate statistical significance. $^{*}P < 0.05$, $^{**}P < 0.01$. (**C**) Metabolome analysis was conducted using WT and xCT-KO PMs stimulated with LPS for 0, 8, and 24 h. Volcano plots of metabolites in xCT-KO vs. WT PMs at indicated time after the treatment with 100 ng/μL LPS (n = 3 for each genotype). Sulfur metabolites are shown in yellow. Green vertical lines denote fold change = 1.5 or 1/1.5, while horizontal lines denote *P*-value = 0.05. *P*-values were calculated by Student's t-test. (**D-F**) Relative abundance of individual sulfur metabolites shown in the right panel of (**C**). Cysteine and its oxidized forms (**D**), glutathione and its precursor (**E**), and transsulfuration pathway metabolites (**F**) are shown. Error bars represent S.E.M. of biological triplicates. Two-way ANOVA was conducted to evaluate statistical significance. $^{*}P < 0.05$, $^{**}P < 0.01$, $^{***}P < 0.001$, $^{****}P < 0.0001$. (For interpretation of the references to colour in this figure legend, the reader is referred to the Web version of this article.)

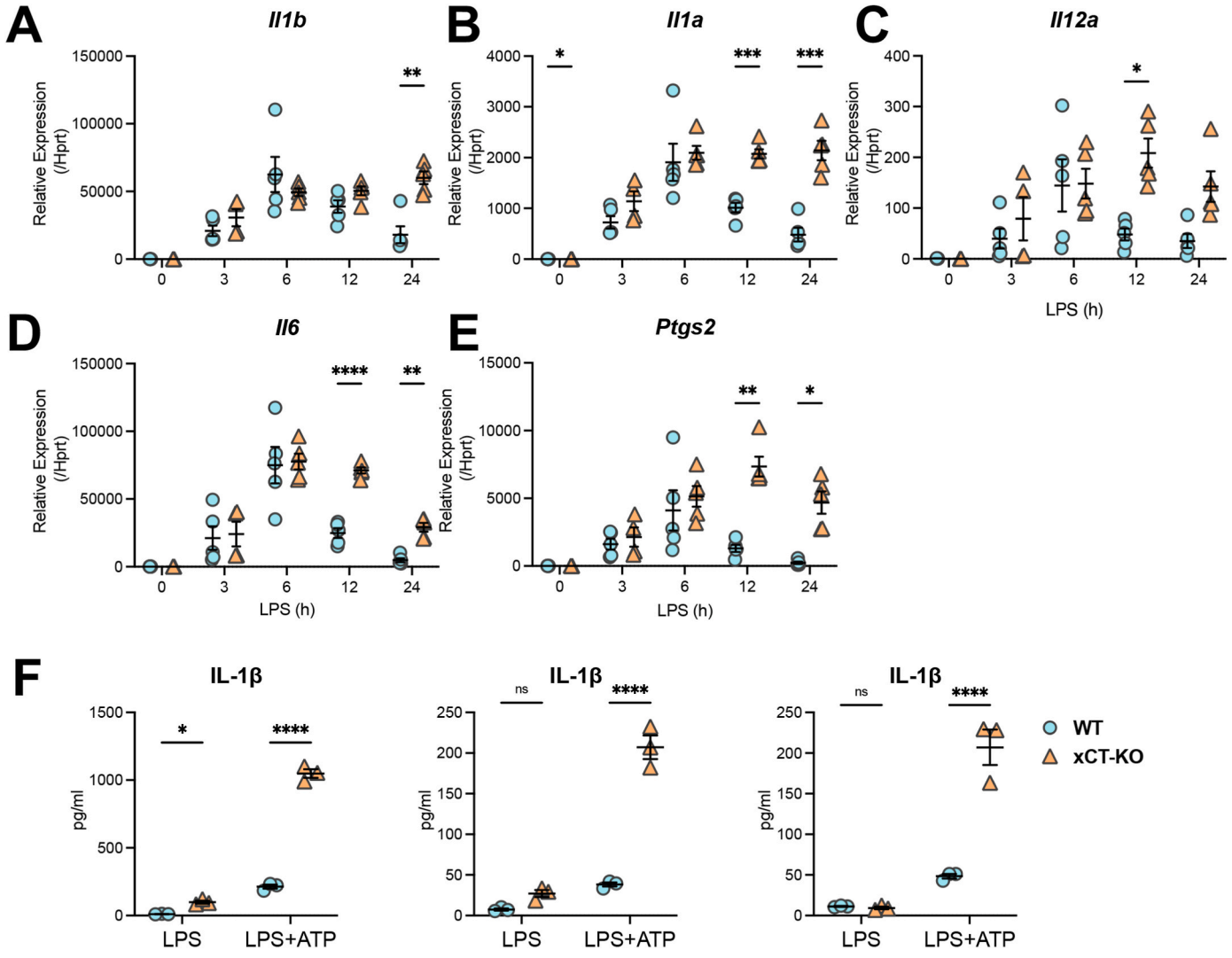

Fig. 3. Enhanced pro-inflammatory phenotypes of xCT-KO PMs.
(**A-E**) RT-PCR quantification of mRNA levels of *Il1b* (**A**), *Il1a* (**B**), *Il12a* (**C**), *Il6* (**D**), and *Ptgs2* (**E**) in WT and xCT-KO PMs stimulated with 100 ng/μl LPS for indicated time (n = 4–5). Error bars represent S.E.M. of 4–5 replicates. Two-way ANOVA was conducted to evaluate statistical significance. $^{*}P < 0.05$, $^{**}P < 0.01$, $^{***}P < 0.001$, $^{****}P < 0.0001$.
(**F**) ELISA quantification of IL-1β in the culture medium after 24 h of LPS treatment followed by 2 h of ATP exposure. Error bars represent S.E.M. of technical triplicates. Results of 3 independent experiments are shown. Two-way ANOVA was conducted to evaluate statistical significance. $^{*}P < 0.05$, $^{****}P < 0.0001$.

of macrophages and causes the failure to terminate the pro-inflammatory response.

3.5. Inhibition of glutathione synthesis does not augment pro-inflammatory response

We asked a question about how taken-up cystine controlled the inflammatory response. Cystine is intracellularly reduced to cysteine, which flows into anabolic and catabolic pathways. Among them, we expected that glutathione synthesis was involved in the control of pro-inflammatory cytokine production as glutathione is the most abundant cysteine-derived metabolite and is implicated to have a role in radical scavenging activity [27,28]. We treated PMs with Buthionine sulphoximine (BSO), an inhibitor of gamma-glutamylcysteine synthetase (γGCS), which is an enzyme required in the rate-limiting step of glutathione synthesis. BSO treatment ablated the intracellular glutathione, with a significant decrease to almost the detection limit at 24 h after the LPS treatment (Fig. 5A). Contrary to our expectation, expression levels

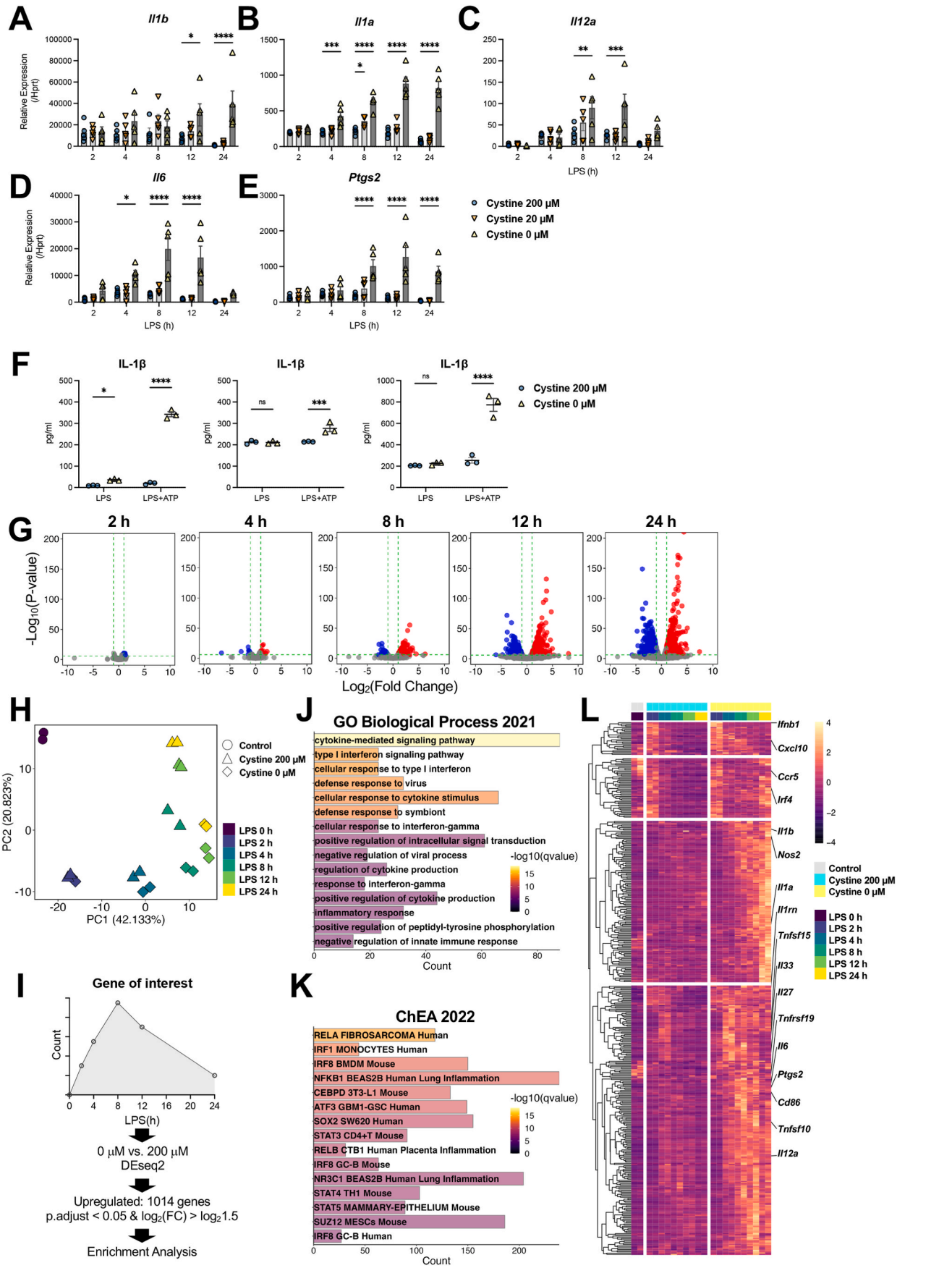

(caption on next page)

Fig. 4. Enhanced pro-inflammatory phenotypes of cystine-depleted PMs.
(**A-E**) RT-PCR quantification of mRNA levels of *Il1b* (**A**), *Il1a* (**B**), *Il12a* (**C**), *Il6* (**D**), and *Ptgs2* (**E**) in PMs stimulated with 100 ng/μl LPS in the culture medium containing different concentration of cystine for the indicated time (n = 5). Error bars represent S.E.M. of 5 replicates. Two-way ANOVA was conducted to evaluate statistical significance. $^{*}P < 0.05$, $^{**}P < 0.01$, $^{***}P < 0.001$, $^{****}P < 0.0001$.
(**F**) ELISA quantification of IL-1β in the culture medium after 24 h of LPS treatment and cystine limitation/depletion followed by 2 h of ATP exposure. Error bars represent the S.E.M. of technical triplicates. Results of 3 independent experiments are shown. Two-way ANOVA was conducted to evaluate statistical significance. $^{*}P < 0.05$, $^{****}P < 0.0001$.
(**G**) Volcano plots of TPM values of RNA-seq data from biological duplicates. TPM values are plotted in the absence vs. presence of cystine at the indicated time after the 100 ng/μl LPS treatment. Upregulated and downregulated genes are shown in red and blue, respectively. Green vertical lines denote fold change = 2 or 1/2, while the horizontal line denotes P-value = 10^{-6}. *P*-values were calculated by Student's t-test.
(**H**) Principal component analysis of RNA-seq data. PMs were exposed to cystine-free medium or cystine-containing (200 μM) medium upon LPS treatment. Control indicates PMs cultured in the medium containing 200 μM without LPS (LPS 0 h).
(**I**) Selection of genes subjected to enrichment analysis. For each gene from the individual sample, AUC was calculated from the TPM values of 6 time points. AUC data were subjected to Deseq2 analysis to identify significantly deviated genes. Genes whose $\log_2$FC (cystine 0 μM vs. 200 μM) > $\log_2$1.5 and adjusted P-value <0.05 were defined as "Upregulated genes." 1014 "Upregulated genes" are then subjected to enrichment analysis.
(**J, K**) Top-hit terms from "GO Biological Process" (**J**) and "ChEA 2022" (**K**) databases.
(**L**) Heatmap visualizing the expression profiles of "Upregulated genes." Representative cytokines and other pro-inflammatory genes are indicated. (For interpretation of the references to colour in this figure legend, the reader is referred to the Web version of this article.)

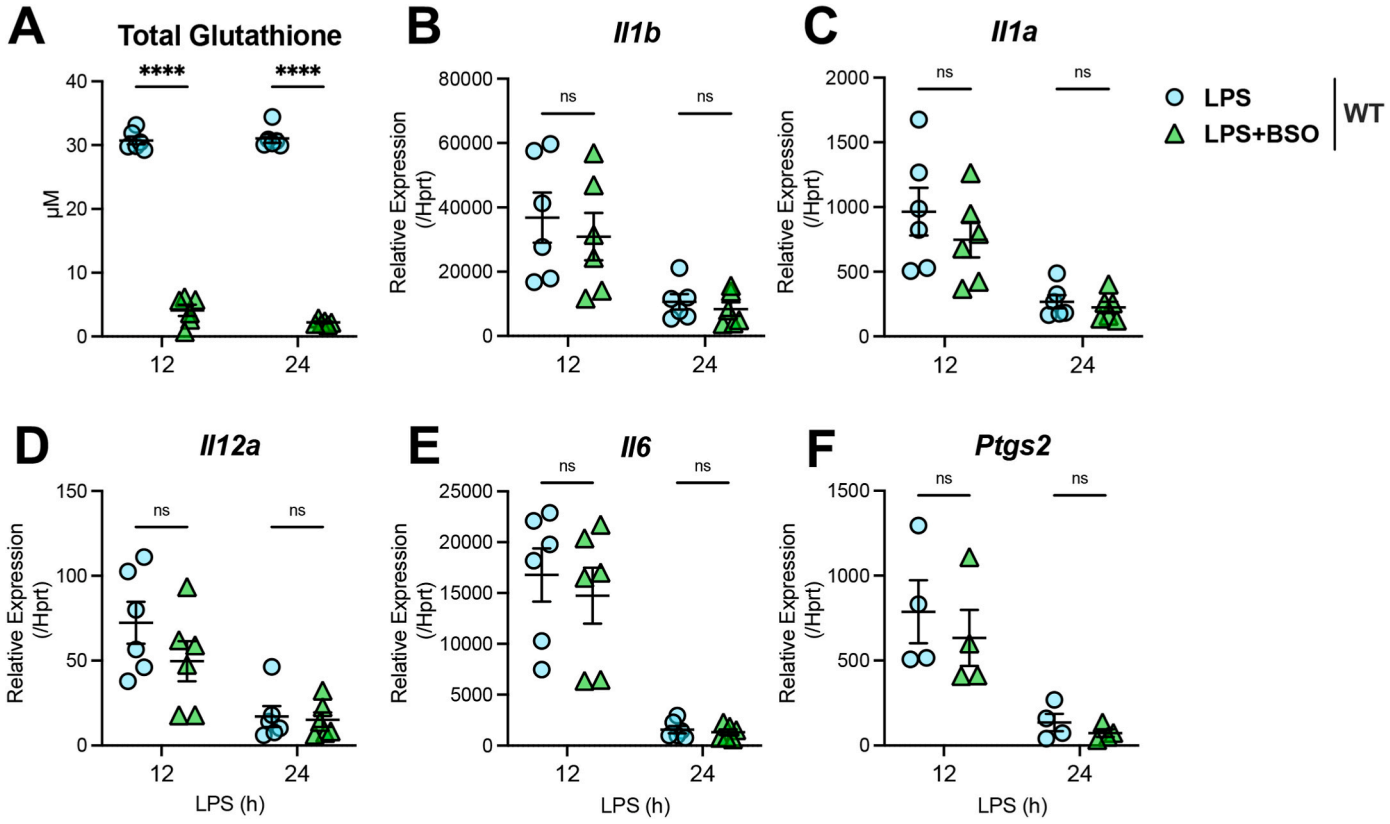

Fig. 5. Glutathione depletion does not augment pro-inflammatory response.
(**A**) Total glutathione concentration in PMs cultured in a medium containing 100 ng/μl LPS in the presence or absence of 100 μM BSO for the indicated time.
(**B–F**) RT-PCR quantification of mRNA levels of *Il1b* (**B**), *Il1a* (**C**), *Il12a* (**D**), *Il6* (**E**), and *Ptgs2* (**F**) in PMs treated in the same way as in (**A**). Error bars represent S.E.M. of 6 replicates. Two-way ANOVA was conducted to evaluate statistical significance. $^{****}P < 0.0001$, ns: not significant.

of *Il1b*, *Il1a*, *IL12a*, *Il6*, and *Ptgs2* were all comparable irrespective of the BSO treatment, indicating that glutathione depletion alone does not augment pro-inflammatory gene expression (Fig. 5B-F). These data demonstrated that increased pro-inflammatory gene expression in cystine-depleted and xCT-KO PMs is not ascribed to the loss of glutathione.

3.6. Detailed profiling of sulfur metabolites reveals the alteration in supersulfide production in xCT-KO macrophages

These data implied the alternative mechanism by which sulfur metabolites control inflammation. Because recent reports demonstrated the important roles of supersulfides, which are synthesized from cysteine, in various biological processes, including inflammation control [18,29,30], we investigated the contribution of supersulfides to our experimental settings. We employed a previously established mass spectrometric quantification method for sulfur metabolites, including supersulfides [17,18], which utilizes β-(4-hydroxyphenyl) ethyl iodoacetamide (HPE-IAM) as a protecting reagent for hydropersulfide moieties. As expected from our metabolomic data, cysteine and reduced/oxidized glutathione were upregulated following LPS treatment, and those changes were utterly absent in xCT-KO PMs (Fig. 6A-D). Cysteine persulfide exhibited almost a similar pattern to that of cysteine (Fig. 6E). Glutathione hydropersulfide and glutathione hydrotrisulfide

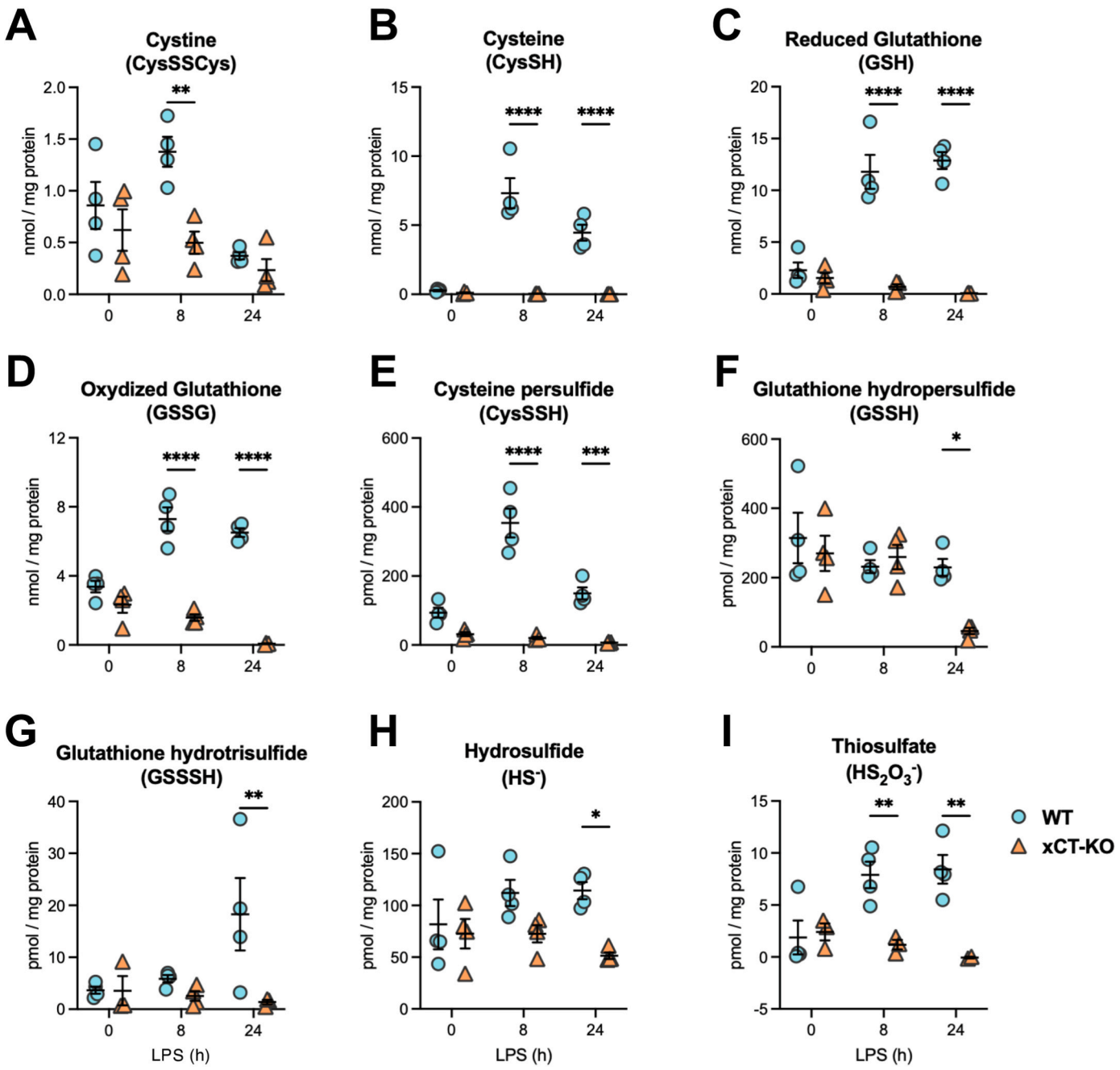

Fig. 6. Sulfur metabolome analysis of macrophages after LPS treatment.
Sulfur metabolites were quantified using WT and xCT-KO PMs cultured in a medium containing 100 ng/μL LPS for indicated time. Cystine (**A**), cysteine (**B**), reduced glutathione (**C**), oxidized glutathione (**D**), cysteine persulfide (**E**), glutathione hydropersulfide (**F**), glutathione hydrotrisulfide (**G**), hydrosulfide (**H**), and thiosulfate (**I**) are shown. Error bars represent S.E.M. of 4 replicates. Two-way ANOVA was conducted to evaluate statistical significance. $^{*}P < 0.05$, $^{**}P < 0.01$, $^{***}P < 0.001$, $^{****}P < 0.0001$.

were significantly decreased in xCT-KO PMs 24 h after the LPS treatment (Fig. 6F and G). Hydrosulfide (HS^-) and thiosulfate ($HS_2O_3^-$), which are regarded as degradative and catabolically oxidized products of supersulfides, respectively [18], were also significantly decreased in xCT-KO PMs.

To further characterize the alteration of sulfur metabolism, we quantified sulfur metabolites in culture supernatants of WT and xCT-KO PMs. The culture supernatants of xCT-KO PMs contained levels of all sulfur metabolites comparable to those measured in the fresh medium without macrophages (Fig. 7), indicating the absence of sulfur metabolites entering or leaving xCT-KO PMs. Cystine (CysSSCys) in the culture media of WT PMs was significantly reduced but not in those of xCT-KO PMs, indicating the cystine consumption by the macrophages via xCT during the inflammatory response (Fig. 7A). Cystine trisulfide (CysSSSCys) showed a similar pattern, implying that cystine trisulfide consumption also relies on xCT activity (Fig. 7B). In the culture media of WT PMs, but not in those of xCT-KO PMs, CysSH, CysSSH, GSH, GSSH, GSSG, and $HS_2O_3^-$ were increased during the inflammatory response, suggesting the presence of secretory mechanism of the sulfur metabolites from macrophages [31] (Fig. 7C-H). Changes in HS^- concentration were negligible (Fig. 7I). Collectively, our sulfur metabolome analysis suggested that the inflammatory response of macrophages is accompanied by increased production of supersulfides from taken-up cystine and increased oxidative catabolism of supersulfides leading to excretion of

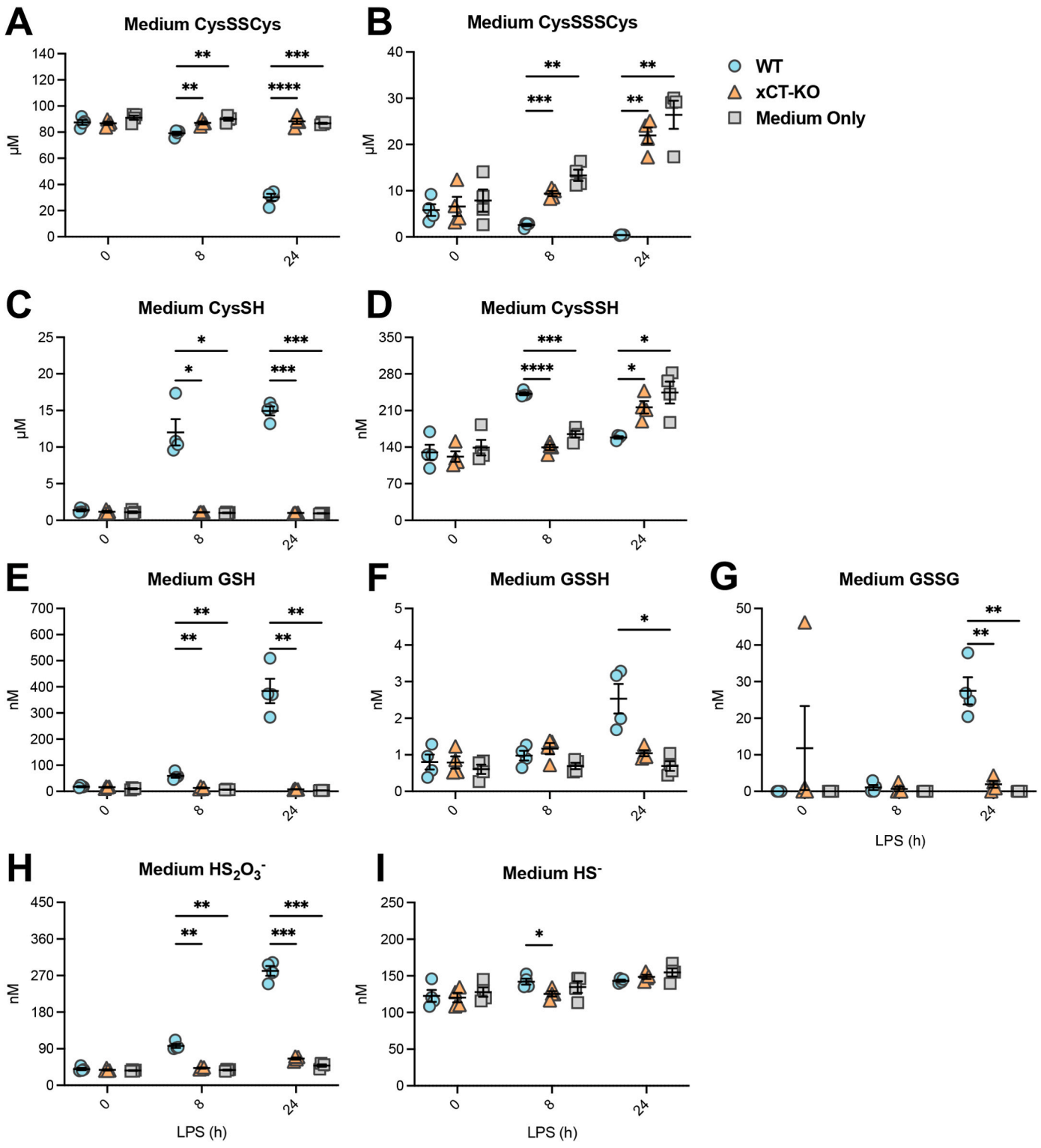

Fig. 7. Sulfur metabolome analysis of culture supernatants of macrophages after LPS treatment.
Sulfur metabolites were quantified using culture supernatants of WT and xCT-KO PMs stimulated with 100 ng/μL LPS for indicated time. Cystine (**A**), cystine trisulfide (**B**), cysteine (**C**), cysteine persulfide (**D**), reduced glutathione (**E**), glutathione hydropersulfide (**F**), oxidized glutathione (**G**), thiosulfate (**H**), and hydrosulfide (**I**) are shown. Fresh medium incubated at the same condition without cells is shown as a negative control (Medium only). Error bars represent S.E.M. of 4 replicates. Two-way ANOVA was conducted to evaluate statistical significance. $^*P < 0.05$, $^{**}P < 0.01$, $^{***}P < 0.001$, $^{****}P < 0.0001$.

thiosulfate, which are all absent in xCT-KO PMs.

3.7. Supplementation of supersulfides cancels the augmented pro-inflammatory mediator expression in xCT-KO PMs

Supersulfide donors, such as glutathione trisulfide and N-

acetylcysteine tetrasulfide (NAC-S2), have been developed to increase intracellular supersulfide levels. A previous study demonstrated that NAC-S2 donates their sulfane sulfur atoms to acceptor thiols via a nucleophilic attack by reduced thiols, producing supersulfides in cells without affecting the abundance of cysteine [19]. We utilized NAC-S2 to examine the modulatory capacity of supersulfides in our experimental setting (Fig. 8A). Strikingly, expression levels of pro-inflammatory cytokines and a mediator, namely, *Il1b*, *Il1a*, *Il12a*, *Il6*, and *Ptgs2*, were significantly suppressed at 12 h after LPS treatment (Fig. 8B-F). Expression levels of *Il1b*, *Il1a*, and *Il12a* were also significantly suppressed at 24 h, while *Il6* and *Ptgs2* remained unaltered. Importantly, an oxidized form of N-acetylcysteine (oxNAC), which does not harbor sulfane sulfurs (Fig. 8A), did not cancel the elevation of the pro-inflammatory gene expression in xCT-KO PMs (Fig. 8B-F). Similarly, glutathione trisulfide (GSSSG) was effective for the attenuation of the pro-inflammatory gene expression in xCT-KO PMs, whereas glutathione disulfide (GSSG) was not (data not shown). These data clearly showed that the loss of supersulfide production is one of the causes for pro-inflammatory phenotypes of macrophages that are unable to utilize extracellular cystine during the inflammatory response. Thus, the increased demand for cysteine in macrophages during the inflammatory response supports the production of supersulfides, which promotes resolution of inflammation, creating a negative feedback loop to prevent an excessive inflammatory response.

4. Discussion

A bunch of dedicated studies have unveiled the dynamic metabolic alterations in immune cells, including macrophages [32–34]. Our results, showing the substantial increase of itaconate and succinate in macrophages following LPS treatment, are well aligned with previous studies describing that LPS stimulation accumulates itaconate via alteration of TCA cycle enzymes, leading to the inhibition of succinate dehydrogenase activity and accumulation of succinate [7,8,35]. Besides, our present study demonstrated that sulfur metabolism supported by xCT is another critical axis regulating macrophage behavior to limit excessive pro-inflammatory gene expression. The cystine uptake by macrophages via xCT is abruptly increased upon LPS treatment, followed by increased production of supersulfides, without which resolution of macrophage inflammatory response is hampered. Here we

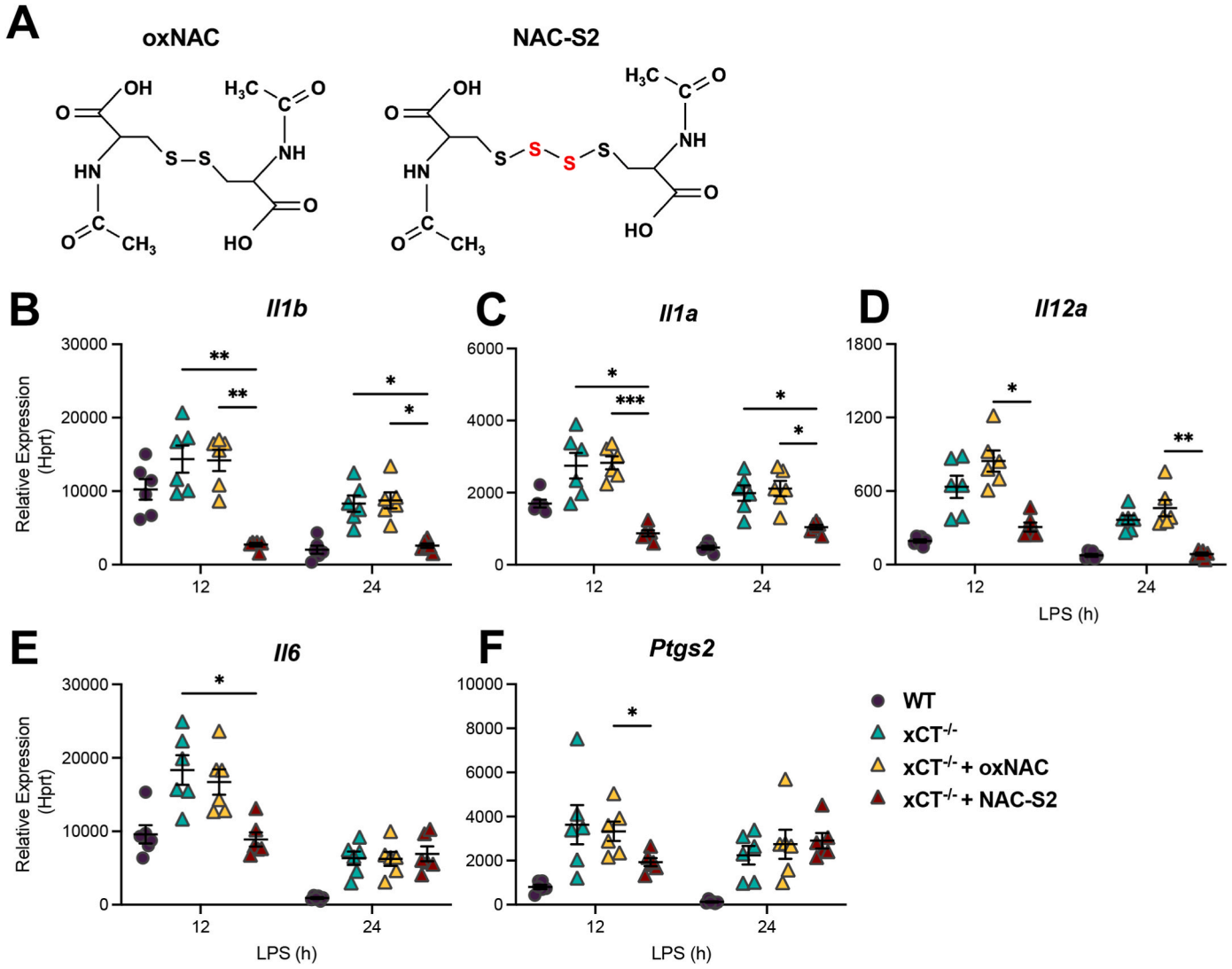

Fig. 8. NAC-S2 cancels augmented inflammatory gene expression in xCT-KO PMs.
(**A**) Chemical structures of oxNAC and NAC-S2. Sulfane sulfur atoms in NAC-S2 are indicated in red. (**B**–**F**) RT-PCR quantification of mRNA levels of *Il1b* (**B**), *Il1a* (**C**), *Il12a* (**D**), *Il6* (**E**), and *Ptgs2* (**F**) in WT or xCT-KO PMs cultured in a medium containing 100 ng/μL LPS in the presence or absence of oxNAC (50 μM) or NAC-S2 (50 μM) for the indicated time. Error bars represent S.E.M. of 6 replicates. Two-way ANOVA was conducted to evaluate statistical significance. $^{*}P < 0.05$, $^{**}P < 0.01$, $^{***}P < 0.001$. (For interpretation of the references to colour in this figure legend, the reader is referred to the Web version of this article.)

propose "sulfur negative feedback loop" that regulates the inflammatory response of macrophages.

Expression of xCT is generally maintained low in basal conditions across organs, but it is strongly induced once exposed to various stimuli [22,36–38], suggesting a critical role of xCT in the stress response. Because cysteine is a building block of glutathione, cysteine supply via xCT in the form of cystine is expected to be required for antioxidant function. Consistently, xCT expression is induced as a part of the NRF2-driven antioxidant pathway in activated macrophages. In LPS-challenged macrophages, accumulated itaconate alkylates KEAP1, resulting in the stabilization of NRF2 [9]. NRF2 then translocates into the nucleus and transcribes the battery of cytoprotective genes, including *Slc7a11* (encoding xCT) and enzymes related to glutathione synthesis, such as *Gclc*, *Gclm*, and *Gss* [39]. Considering the synchronized activities of cystine uptake and glutathione synthesis, we initially expected that cystine would inhibit excessive pro-inflammatory reactions by enhancing glutathione synthesis. Indeed, glutathione is generally regarded to protect cells from toxicity by counteracting radicals, and the glutathione system is reported to coordinate macrophage functions and polarization patterns [40–42]. Contrary to our expectations, however, BSO treatment in WT PMs did not increase pro-inflammatory gene expression, albeit successful glutathione reduction by more than 90% efficacy. In the previous study, BSO treatment in RAW264.7 cells did not augment inflammatory cytokine expression but downregulated *Il1b* expression when stimulated with LPS for 2 h [40]. Our results resemble this observation and thus emphasize that endogenous glutathione does not strikingly control the cytokine expression, at least at a transcriptional level.

Supersulfides are present in the form of low-molecular-weight metabolites as well as proteins with per-/poly-sulfidated cysteine residues [17,18,30,43–45]. A previous study demonstrated that supersulfide supplementation limits the pro-inflammatory cytokine expression via impeding TLR signaling [19]. However, whether endogenously produced supersulfides have any regulatory roles remained unclear. Our present study demonstrated for the first time that activated macrophages produce supersulfides depending on the cystine uptake via xCT and that blockade of the cystine uptake augmented pro-inflammatory gene expression in xCT-KO PMs, which was restored by supplementation of NAC-S2, a supersulfide donor, suggesting that endogenous supersulfides serve as cell-intrinsic signals to terminate pro-inflammatory reactions. While CBS, CGL, 3-mercapto pyruvate sulfurtransferase (3-MST), cysteinyl-tRNA synthetase 1 (CARS1), and cysteinyl-tRNA synthetase 2 (CASR2) have been identified as supersulfide synthesizing enzymes [46], which of them makes a major contribution to the supersulfide synthesis in macrophages needs further investigation.

How supersulfide decrease results in the augmentation of pro-inflammatory reactions is unclear, but we propose two possibilities. Considering the potent radical scavenging activity due to the superior reactivity to corresponding thiols [18,47], supersulfide increase by NAC-S2 may decrease reactive oxygen species (ROS) in LPS-stimulated macrophages. Since ROS augments pro-inflammatory cytokine production via NF-κB signaling and HIF-1α [48,49], quenching ROS by NAC-S2 could be a mechanism to attenuate inflammation. Another possibility is the supersulfidation of protein cysteine residues. Protein supersulfidation alters the protein function, coordinating multiple cellular processes, including oxidative stress, endoplasmic stress, and autophagy [50,51]. Supplementation of NAC polysulfides may increase protein supersulfidation either by direct modification of protein thiols or by formation of low-molecular-weight supersulfides such as cysteine persulfides [19]. Considering that inflammatory response, including NF-kB activation, is modulated through posttranslational thiol modifications [52], it is worthwhile examining the supersulfidation of proteins that are involved in cytokine production.

Although NAC-S2 treatment restored all examined pro-inflammatory gene expressions at 12 h after LPS treatment in xCT-KO macrophages, we did not see any effects for some of the genes at 24 h. We reasoned that this might be due to the elevated asparagine synthesis by enhanced ATF4 activity, as a recent report demonstrated that asparagine positively controls IL-1β production in macrophages [53]. Indeed, ATF4 protein was significantly increased in the nucleus of xCT-KO PMs, accompanied by *Asns* upregulation and asparagine accumulation. It is plausible that the enhanced pro-inflammatory response in xCT-KO PMs involves a combination of mechanisms, including the insufficiency of supersulfides and ATF4-mediated amino acid starvation response.

In summary, these results elucidate that xCT-mediated cystine uptake elicits a cell-intrinsic signal to restrain excessive pro-inflammatory response via supersulfide production. This would imply that an approach to facilitate cystine accumulation is beneficial to control pro-inflammatory reactions and prevent oxidative damage to tissues. However, previous *in vivo* studies using systemic xCT-KO mice yielded contradictory results, such as exacerbation of hepatocellular injury in APAP-treated mice [36], overproduction of IL-1β, IL-6, and TNFα after subcutaneous injection of 3-methylcholanthrene [23] and amelioration of peripheral and central inflammation and behavioral outcomes in LPS-induced depressive mouse model [54], implying the role of xCT varies depending on different cellular and tissue contexts. Nevertheless, macrophage-specific xCT knockout limit tumorigenicity and metastasis in several cancer models by blocking M2-type polarization [55,56], which strongly suggests that the role of cystine uptake in macrophages is anti-inflammatory. Further studies need to be conducted to clarify the tissue- and cell-specific role of xCT.

Author contributions

H.T. designed the study, conducted the experiments, and wrote the paper. S.M. conducted the sulfur mass spectrometry analysis and wrote the paper. Z.L. conducted the primary culture experiments. T.S., T.A. and H. Sato provided critical materials and methods and interpreted the data. M.T., Y.I. and T.B. conducted the metabolomic analysis. H. Sekine and H.M. designed the study, supervised the research, and wrote the paper.

Declaration of competing interest

The authors declare no competing financial or nonfinancial interests.

Data availability

I have shared the link to our data in the main text.

Acknowledgments

We thank the Biomedical Research Core of the Institute of Development, Aging and Cancer for their technical support. We are also grateful to the technical staff members (A. Hidaka, N. Seki, and M. Goto) of Kyushu University for their technical support. The graphical abstract was created with BioRender.com.

This work was supported by JSPS grant numbers 17H06299 (T.B.), 21H02071 (T.S.), 21H05267 (T.S.), 23H02672 (H.Sekine), 21H05258 (T.S., T.A. and H.M.), 21H05263 (T.A.), 21H05264 (H.M.), and 21H04799 (H.M.), JST A-STEP JPMJTR204J (T.B.), and the Medical Research Center Initiative for High Depth Omics Program of the Medical Institute of Bioregulation, Kyushu University (T.B.). The funders had no role in the study design, data collection and analysis, decision to publish or manuscript preparation.

Appendix A. Supplementary data

Supplementary data to this article can be found online at https://doi.org/10.1016/j.redox.2023.102834.

References

[1] T.A. Wynn, A. Chawla, J.W. Pollard, Macrophage biology in development, homeostasis and disease, Nature 496 (7446) (2013) 445–455, https://doi.org/10.1038/NATURE12034.

[2] P.J. Murray, T.A. Wynn, Protective and pathogenic functions of macrophage subsets, Nat. Rev. Immunol. 11 (11) (2011) 723–737, https://doi.org/10.1038/NRI3073.

[3] C. Nathan, A. Ding, Nonresolving inflammation, Cell 140 (6) (2010) 871–882, https://doi.org/10.1016/J.CELL.2010.02.029.

[4] L.A.J. O'neill, Glycolytic reprogramming by TLRs in dendritic cells, Nat. Immunol. 15 (4) (2014) 314–315, https://doi.org/10.1038/NI.2852.

[5] M. Bambouskova, L. Gorvel, V. Lampropoulou, A. Sergushichev, E. Loginicheva, K. Johnson, D. Korenfeld, M.E. Mathyer, H. Kim, L.H. Huang, D. Duncan, H. Bregman, A. Keskin, A. Santeford, R.S. Apte, R. Sehgal, B. Johnson, G. K. Amarasinghe, M.P. Soares, M.N. Artyomov, Electrophilic properties of itaconate and derivatives regulate the IκBζ-ATF3 inflammatory axis, Nature 556 (7702) (2018) 501–504, https://doi.org/10.1038/S41586-018-0052-Z.

[6] A. Hooftman, S. Angiari, S. Hester, S.E. Corcoran, M.C. Runtsch, C. Ling, M. C. Ruzek, P.F. Slivka, A.F. McGettrick, K. Banahan, M.M. Hughes, A.D. Irvine, R. Fischer, L.A.J. O'Neill, The immunomodulatory metabolite itaconate modifies NLRP3 and inhibits inflammasome activation, Cell Metabol. 32 (3) (2020) 468–478.e7, https://doi.org/10.1016/J.CMET.2020.07.016.

[7] V. Lampropoulou, A. Sergushichev, M. Bambouskova, S. Nair, E.E. Vincent, E. Loginicheva, L. Cervantes-Barragan, X. Ma, S.C.C. Huang, T. Griss, C. J. Weinheimer, S. Khader, G.J. Randolph, E.J. Pearce, R.G. Jones, A. Diwan, M. S. Diamond, M.N. Artyomov, Itaconate links inhibition of succinate dehydrogenase with macrophage metabolic remodeling and regulation of inflammation, Cell Metabol. 24 (1) (2016) 158–166, https://doi.org/10.1016/J.CMET.2016.06.004.

[8] E.L. Mills, B. Kelly, A. Logan, A.S.H. Costa, M. Varma, C.E. Bryant, P. Tourlomousis, J.H.M. Däbritz, E. Gottlieb, I. Latorre, S.C. Corr, G. McManus, D. Ryan, H.T. Jacobs, M. Szibor, R.J. Xavier, T. Braun, C. Frezza, M.P. Murphy, L.A. O'Neill, Succinate dehydrogenase supports metabolic repurposing of mitochondria to drive inflammatory macrophages, Cell 167 (2) (2016) 457–470.e13, https://doi.org/10.1016/J.CELL.2016.08.064.

[9] E.L. Mills, D.G. Ryan, H.A. Prag, D. Dikovskaya, D. Menon, Z. Zaslona, M. P. Jedrychowski, A.S.H. Costa, M. Higgins, E. Hams, J. Szpyt, M.C. Runtsch, M. S. King, J.F. McGouran, R. Fischer, B.M. Kessler, A.F. McGettrick, M.M. Hughes, R. G. Carroll, L.A. O'Neill, Itaconate is an anti-inflammatory metabolite that activates Nrf2 via alkylation of KEAP1, Nature 556 (7699) (2018) 113–117, https://doi.org/10.1038/NATURE25986.

[10] W. Qin, K. Qin, Y. Zhang, W. Jia, Y. Chen, B. Cheng, L. Peng, N. Chen, Y. Liu, W. Zhou, Y.L. Wang, X. Chen, C. Wang, S-glycosylation-based cysteine profiling reveals regulation of glycolysis by itaconate, Nat. Chem. Biol. 15 (10) (2019) 983–991, https://doi.org/10.1038/S41589-019-0323-5.

[11] G.M. Tannahill, A.M. Curtis, J. Adamik, E.M. Palsson-Mcdermott, A.F. McGettrick, G. Goel, C. Frezza, N.J. Bernard, B. Kelly, N.H. Foley, L. Zheng, A. Gardet, Z. Tong, S.S. Jany, S.C. Corr, M. Haneklaus, B.E. Caffrey, K. Pierce, S. Walmsley, L.A. J. O'Neill, Succinate is an inflammatory signal that induces IL-1β through HIF-1α, Nature 496 (7444) (2013) 238–242, https://doi.org/10.1038/NATURE11986.

[12] B.B. Mishra, V.A.K. Rathinam, G.W. Martens, A.J. Martinot, H. Kornfeld, K. A. Fitzgerald, C.M. Sassetti, Nitric oxide controls the immunopathology of tuberculosis by inhibiting NLRP3 inflammasome-dependent processing of IL-1β, Nat. Immunol. 14 (1) (2013) 52–60, https://doi.org/10.1038/NI.2474.

[13] B. Everts, E. Amiel, G.J.W. Van Der Windt, T.C. Freitas, R. Chott, K.E. Yarasheski, E.L. Pearce, E.J. Pearce, Commitment to glycolysis sustains survival of NO-producing inflammatory dendritic cells, Blood 120 (7) (2012) 1422–1431, https://doi.org/10.1182/BLOOD-2012-03-419747.

[14] A.E. Rodriguez, G.S. Ducker, L.K. Billingham, C.A. Martinez, N. Mainolfi, V. Suri, A. Friedman, M.G. Manfredi, S.E. Weinberg, J.D. Rabinowitz, N.S. Chandel, Serine metabolism supports macrophage IL-1β production, Cell Metabol. 29 (4) (2019) 1003–1011.e4, https://doi.org/10.1016/J.CMET.2019.01.014.

[15] S. Bannai, E. Kitamura, Transport interaction of L-cystine and L-glutamate in human diploid fibroblasts in culture, J. Biol. Chem. 255 (6) (1980) 2372–2376, https://doi.org/10.1016/s0021-9258(19)85901-x.

[16] H. Sato, M. Tamba, T. Ishii, S. Bannai, Cloning and expression of a plasma membrane cystine/glutamate exchange transporter composed of two distinct proteins, J. Biol. Chem. 274 (17) (1999) 11455–11458, https://doi.org/10.1074/JBC.274.17.11455.

[17] T. Akaike, T. Ida, F.Y. Wei, M. Nishida, Y. Kumagai, M.M. Alam, H. Ihara, T. Sawa, T. Matsunaga, S. Kasamatsu, A. Nishimura, M. Morita, K. Tomizawa, A. Nishimura, S. Watanabe, K. Inaba, H. Shima, N. Tanuma, M. Jung, H. Motohashi, Cysteinyl-tRNA synthetase governs cysteine polysulfidation and mitochondrial bioenergetics, Nat. Commun. 8 (1) (2017), https://doi.org/10.1038/S41467-017-01311-Y.

[18] T. Ida, T. Sawa, H. Ihara, Y. Tsuchiya, Y. Watanabe, Y. Kumagai, M. Suematsu, H. Motohashi, S. Fujii, T. Matsunaga, M. Yamamoto, K. Ono, N.O. Devarie-Baez, M. Xian, J.M. Fukuto, T. Akaike, Reactive cysteine persulfides and S-polythiolation regulate oxidative stress and redox signaling, Proc. Natl. Acad. Sci. U. S. A. 111 (21) (2014) 7606–7611, https://doi.org/10.1073/PNAS.1321232111/-/DCSUPPLEMENTAL/SAPP.PDF.

[19] T. Zhang, K. Ono, H. Tsutsuki, H. Ihara, W. Islam, T. Akaike, T. Sawa, Enhanced cellular polysulfides negatively regulate TLR4 signaling and mitigate lethal endotoxin shock, Cell Chem. Biol. 26 (5) (2019) 686–698.e4, https://doi.org/10.1016/J.CHEMBIOL.2019.02.003.

[20] A. Nishimura, K. Shimoda, T. Tanaka, T. Toyama, K. Nishiyama, Y. Shinkai, T. Numaga-Tomita, D. Yamazaki, Y. Kanda, T. Akaike, Y. Kumagai, M. Nishida, Depolysulfidation of Drp1 induced by low-dose methylmercury exposure increases cardiac vulnerability to hemodynamic overload, Sci. Signal. 12 (587) (2019), https://doi.org/10.1126/SCISIGNAL.AAW1920/SUPPL_FILE/AAW1920_SM.PDF.

[21] M.M. Alam, A. Kishino, E. Sung, H. Sekine, T. Abe, S. Murakami, T. Akaike, H. Motohashi, Contribution of NRF2 to sulfur metabolism and mitochondrial activity, Redox Biol. 60 (2023), https://doi.org/10.1016/J.REDOX.2023.102624.

[22] S. Kobayashi, S. Hamashima, T. Homma, M. Sato, R. Kusumi, S. Bannai, J. Fujii, H. Sato, Cystine/glutamate transporter, system xc-, is involved in nitric oxide production in mouse peritoneal macrophages, Nitric Oxide : Biology and Chemistry 78 (2018) 32–40, https://doi.org/10.1016/J.NIOX.2018.05.005.

[23] A. Nabeyama, A. Kurita, K. Asano, Y. Miyake, T. Yasuda, I. Miura, G. Nishitai, S. Arakawa, S. Shimizu, S. Wakana, H. Yoshida, M. Tanaka, xCT deficiency accelerates chemically induced tumorigenesis, Proc. Natl. Acad. Sci. U. S. A. 107 (14) (2010) 6436–6441, https://doi.org/10.1073/PNAS.0912827107.

[24] H. Sato, A. Shiiya, M. Kimata, K. Maebara, M. Tamba, Y. Sakakura, N. Makino, F. Sugiyama, K.I. Yagami, T. Moriguchi, S. Takahashi, S. Bannai, Redox imbalance in cystine/glutamate transporter-deficient mice, J. Biol. Chem. 280 (45) (2005) 37423–37429, https://doi.org/10.1074/JBC.M506439200.

[25] T. Fushimi, Y. Izumi, M. Takahashi, K. Hata, Y. Murano, T. Bamba, Dynamic metabolome analysis reveals the metabolic fate of medium-chain fatty acids in AML12 cells, J. Agric. Food Chem. 68 (43) (2020) 11997–12010, https://doi.org/10.1021/ACS.JAFC.0C04723.

[26] T. Takata, M. Jung, T. Matsunaga, T. Ida, M. Morita, H. Motohashi, X. Shen, C. G. Kevil, J.M. Fukuto, T. Akaike, Methods in sulfide and persulfide research, Nitric Oxide : Biology and Chemistry 116 (2021) 47–64, https://doi.org/10.1016/J.NIOX.2021.09.002.

[27] R. Brigelius-Flohé, M. Maiorino, Glutathione peroxidases, Biochim. Biophys. Acta 1830 (5) (2013) 3289–3303, https://doi.org/10.1016/J.BBAGEN.2012.11.020.

[28] M. Maiorino, M. Conrad, F. Ursini, GPx4, lipid peroxidation, and cell death: discoveries, rediscoveries, and open issues, Antioxidants Redox Signal. 29 (1) (2018) 61–74, https://doi.org/10.1089/ARS.2017.7115.

[29] S. Fujii, T. Sawa, H. Motohashi, T. Akaike, Persulfide synthases that are functionally coupled with translation mediate sulfur respiration in mammalian cells, Br. J. Pharmacol. 176 (4) (2019) 607–615, https://doi.org/10.1111/BPH.14356.

[30] T. Numakura, H. Sugiura, T. Akaike, T. Ida, S. Fujii, A. Koarai, M. Yamada, K. Onodera, Y. Hashimoto, R. Tanaka, K. Sato, Y. Shishikura, T. Hirano, S. Yanagisawa, N. Fujino, T. Okazaki, T. Tamada, Y. Hoshikawa, Y. Okada, M. Ichinose, Production of reactive persulfide species in chronic obstructive pulmonary disease, Thorax 72 (12) (2017) 1074–1083, https://doi.org/10.1136/THORAXJNL-2016-209359.

[31] T. Zhang, H. Tsutsuki, W. Islam, K. Ono, K. Takeda, T. Akaike, T. Sawa, ATP exposure stimulates glutathione efflux as a necessary switch for NLRP3 inflammasome activation, Redox Biol. 41 (2021), 101930, https://doi.org/10.1016/J.REDOX.2021.101930.

[32] S. Galván-Peña, L.A.J. O'Neill, Metabolic reprograming in macrophage polarization, Front. Immunol. 5 (AUG) (2014), https://doi.org/10.3389/FIMMU.2014.00420.

[33] L.A.J. O'Neill, R.J. Kishton, J. Rathmell, A guide to immunometabolism for immunologists, Nat. Rev. Immunol. 16 (9) (2016) 553–565, https://doi.org/10.1038/NRI.2016.70.

[34] H. Takeda, T. Yamaguchi, H. Yano, J. Tanaka, Microglial metabolic disturbances and neuroinflammation in cerebral infarction, J. Pharmacol. Sci. 145 (1) (2021) 130–139, https://doi.org/10.1016/J.JPHS.2020.11.007.

[35] M.P. Murphy, L.A.J. O'Neill, Krebs cycle reimagined: the emerging roles of succinate and itaconate as signal transducers, Cell 174 (4) (2018) 780–784, https://doi.org/10.1016/J.CELL.2018.07.030.

[36] S. Kobayashi, K. Kuwata, T. Sugimoto, K. Igarashi, M. Osaki, F. Okada, J. Fujii, S. Bannai, H. Sato, Enhanced expression of cystine/glutamate transporter in the lung caused by the oxidative-stress-inducing agent paraquat, Free Radic. Biol. Med. 53 (12) (2012) 2197–2203, https://doi.org/10.1016/j.freeradbiomed.2012.09.040.

[37] S. Maschalidi, P. Mehrotra, B.N. Keçeli, H.K.L. De Cleene, K. Lecomte, R. Van der Cruyssen, P. Janssen, J. Pinney, G. van Loo, D. Elewaut, A. Massie, E. Hoste, K. S. Ravichandran, Targeting SLC7A11 improves efferocytosis by dendritic cells and wound healing in diabetes, Nature 606 (7915) (2022) 776–784, https://doi.org/10.1038/S41586-022-04754-6.

[38] C. Procaccini, S. Garavelli, F. Carbone, D. Di Silvestre, C. La Rocca, D. Greco, A. Colamatteo, M.T. Lepore, C. Russo, G. De Rosa, D. Faicchia, F. Prattichizzo, S. Grossi, P. Campomenosi, F. Buttari, P. Mauri, A. Uccelli, M. Salvetti, V. Brescia Morra, G. Matarese, Signals of pseudo-starvation unveil the amino acid transporter SLC7A11 as key determinant in the control of Treg cell proliferative potential, Immunity 54 (7) (2021) 1543–1560.e6, https://doi.org/10.1016/J.IMMUNI.2021.04.014.

[39] M. Yamamoto, T.W. Kensler, H. Motohashi, The KEAP1-NRF2 system: a thiol-based sensor-effector apparatus for maintaining redox homeostasis, Physiol. Rev. 98 (3) (2018) 1169–1203, https://doi.org/10.1152/PHYSREV.00023.2017.

[40] M. Diotallevi, P. Checconi, A.T. Palamara, I. Celestino, L. Coppo, A. Holmgren, K. Abbas, F. Peyrot, M. Mengozzi, P. Ghezzi, Glutathione fine-tunes the innate immune response toward antiviral pathways in a macrophage cell line independently of its antioxidant properties, Front. Immunol. 8 (SEP) (2017), https://doi.org/10.3389/FIMMU.2017.01239.

[41] P. Ghezzi, Role of glutathione in immunity and inflammation in the lung, Int. J. Gen. Med. 4 (2011) 105–113, https://doi.org/10.2147/IJGM.S15618.

[42] T. Zhang, H. Tsutsuki, W. Islam, K. Ono, K. Takeda, T. Akaike, T. Sawa, ATP exposure stimulates glutathione efflux as a necessary switch for NLRP3

inflammasome activation, Redox Biol. 41 (2021), https://doi.org/10.1016/J.REDOX.2021.101930.
[43] H. Kunikata, T. Ida, K. Sato, N. Aizawa, T. Sawa, H. Tawarayama, N. Murayama, S. Fujii, T. Akaike, T. Nakazawa, Metabolomic profiling of reactive persulfides and polysulfides in the aqueous and vitreous humors, Sci. Rep. 7 (2017), https://doi.org/10.1038/SREP41984.
[44] K. Ono, M. Jung, T. Zhang, H. Tsutsuki, H. Sezaki, H. Ihara, F.Y. Wei, K. Tomizawa, T. Akaike, T. Sawa, Synthesis of l-cysteine derivatives containing stable sulfur isotopes and application of this synthesis to reactive sulfur metabolome, Free Radic. Biol. Med. 106 (2017) 69–79, https://doi.org/10.1016/J.FREERADBIOMED.2017.02.023.
[45] H. Peng, J. Shen, K.A. Edmonds, J.L. Luebke, A.K. Hickey, L.D. Palmer, F.-M. J. Chang, K.A. Bruce, T.E. Kehl-Fie, E.P. Skaar, D.P. Giedroc, Sulfide homeostasis and nitroxyl intersect via formation of reactive sulfur species in Staphylococcus aureus, mSphere 2 (3) (2017), https://doi.org/10.1128/MSPHERE.00082-17/SUPPL_FILE/SPH003172308SF10.PDF.
[46] J.M. Fukuto, L.J. Ignarro, P. Nagy, D.A. Wink, C.G. Kevil, M. Feelisch, M. M. Cortese-Krott, C.L. Bianco, Y. Kumagai, A.J. Hobbs, J. Lin, T. Ida, T. Akaike, Biological hydropersulfides and related polysulfides - a new concept and perspective in redox biology, FEBS (Fed. Eur. Biochem. Soc.) Lett. 592 (12) (2018) 2140–2152, https://doi.org/10.1002/1873-3468.13090.
[47] D. Benchoam, J.A. Semelak, E. Cuevasanta, M. Mastrogiovanni, J.S. Grassano, G. Ferrer-Sueta, A. Zeida, M. Trujillo, M.N. Möller, D.A. Estrin, B. Alvarez, Acidity and nucleophilic reactivity of glutathione persulfide, J. Biol. Chem. 295 (46) (2020) 15466–15481, https://doi.org/10.1074/JBC.RA120.014728.
[48] S. Nakajima, M. Kitamura, Bidirectional regulation of NF-κB by reactive oxygen species: a role of unfolded protein response, Free Radic. Biol. Med. 65 (2013) 162–174, https://doi.org/10.1016/J.FREERADBIOMED.2013.06.020.
[49] A.F. McGettrick, L.A.J. O'Neill, The role of HIF in immunity and inflammation, Cell Metabol. 32 (4) (2020) 524–536, https://doi.org/10.1016/J.CMET.2020.08.002.
[50] M. Jung, S. Kasamatsu, T. Matsunaga, S. Akashi, K. Ono, A. Nishimura, M. Morita, H. Abdul Hamid, S. Fujii, H. Kitamura, T. Sawa, T. Ida, H. Motohashi, T. Akaike, Protein polysulfidation-dependent persulfide dioxygenase activity of ethylmalonic encephalopathy protein 1, Biochem. Biophys. Res. Commun. 480 (2) (2016) 180–186, https://doi.org/10.1016/J.BBRC.2016.10.022.
[51] B. Pedre, U. Barayeu, D. Ezeriņa, T.P. Dick, The mechanism of action of N-acetylcysteine (NAC): the emerging role of H2S and sulfane sulfur species, Pharmacol. Therapeut. 228 (2021), https://doi.org/10.1016/J.PHARMTHERA.2021.107916.
[52] N. Sen, B.D. Paul, M.M. Gadalla, A.K. Mustafa, T. Sen, R. Xu, S. Kim, S.H. Snyder, Hydrogen sulfide-linked sulfhydration of NF-κB mediates its antiapoptotic actions, Mol. Cell 45 (1) (2012) 13–24, https://doi.org/10.1016/J.MOLCEL.2011.10.021.
[53] H. Wang, X. Zheng, B. Liu, Y. Xia, Z. Xin, B. Deng, L. He, J. Deng, W. Ren, Aspartate metabolism facilitates IL-1b production in inflammatory macrophages, Front. Immunol. 12 (2021), 753092, https://doi.org/10.3389/fimmu.2021.753092.
[54] G. Albertini, L. Deneyer, S. Ottestad-Hansen, Y. Zhou, G. Ates, L. Walrave, T. Demuyser, E. Bentea, H. Sato, D. De Bundel, N.C. Danbolt, A. Massie, I. Smolders, Genetic deletion of xCT attenuates peripheral and central inflammation and mitigates LPS-induced sickness and depressive-like behavior in mice, Glia 66 (9) (2018) 1845–1861, https://doi.org/10.1002/GLIA.23343.
[55] B. Tang, Y. Wang, W. Xu, J. Zhu, Q. Weng, W. Chen, S. Fang, Y. Yang, R. Qiu, M. Chen, W. Mao, M. Xu, Z. Zhao, S. Cai, H. Zhang, J. Ji, Macrophage xCT deficiency drives immune activation and boosts responses to immune checkpoint blockade in lung cancer, Cancer Lett. 554 (2023), https://doi.org/10.1016/J.CANLET.2022.216021.
[56] B. Tang, J. Zhu, Y. Wang, W. Chen, S. Fang, W. Mao, Z. Xu, Y. Yang, Q. Weng, Z. Zhao, M. Chen, J. Ji, Targeted xCT-mediated ferroptosis and protumoral polarization of macrophages is effective against HCC and enhances the efficacy of the anti-PD-1/L1 response, Adv. Sci. 10 (2) (2023), https://doi.org/10.1002/advs.202203973.